Supplementary materials

Performance evaluation of THz pulsed imaging system: point spread function, broadband THz beam visualization and image reconstruction

Marta Di Fabrizio [1,*], Annalisa D'Arco[2,*], Sen Mou[2], Luigi Palumbo[3], Massimo Petrarca[2,3] and Stefano Lupi[1,4]

[1] Physics Department, University of Rome 'La Sapienza', Piazzale Aldo Moro 5, 00185 Rome, Italy; stefano.lupi@roma1.infn.it (S.L.)
[2] INFN - Section of Rome 'La Sapienza', P.le Aldo Moro 2, 00185 Rome, Italy; sen.mou@roma1.infn.it (S.M.), massimo.petrarca@uniroma1.it (M.P.)
[3] SBAI-Department of Basic and Applied Sciences for Engineering, Physics, University of Rome 'La Sapienza', Via Scarpa 16, 00161 Rome, Italy; luigi.palumbo@uniroma1.it (L.P.)
[4] INFN- LNF, Via E. Fermi 40, 00044 Frascati, Italy;
* Correspondence: martadifabrizio@gmail.com (M.D.F.), annalisa.darco@roma1.infn.it (A.D.A.)

Here, we report our THz spectroscopic characterization of linen sample and some notes about noise evaluation in the acquired images. In particular, we looked at background noise and signal-to-noise ratio (SNR) using some of the spectral images of the 200 μm pinhole described in Section 4.1.

S1. Spectroscopy theoretical notes

Before acquiring linen images, prior THz spectroscopic measurements have been performed. As seen in Section 2, coherent detection allows both THz electric field amplitude and phase measurement as a function of time. Using the FFT, the spectral distribution of the THz pulse in the frequency domain $\tilde{E}(\omega)$ is derived [1]:

$$\tilde{E}(\omega) = A(\omega)e^{-i\varphi(\omega)} = \int dt\, E(t)e^{-i\omega t} \qquad \text{(S1)}$$

where $\omega = 2\pi f$ is the angular frequency, f is the ordinary frequency, $A(\omega)$ is the spectral amplitude ($A(\omega) = |\tilde{E}(\omega)|$) and $\varphi(\omega)$ the phase. Like in any spectroscopic system, THz spectroscopy is based on changes in the THz power spectrum after transmission through or reflection from a reference R and a selected sample S. By comparing their electric fields $E_R(t)$, $E_S(t)$, and their power spectra $|\tilde{E}_R(\omega)|^2$, $|\tilde{E}_S(\omega)|^2$ many information can be assessed. The transmittance as a function of frequency is given by [1]:

$$T(\omega) = \frac{|\tilde{E}_S(\omega)|^2}{|\tilde{E}_R(\omega)|^2} \qquad \text{(S2)}$$

Figures S1 and S2 show the THz pulse as a function of time and the THz power spectrum as a function of frequency for our THz-TDS system, with no sample inserted in the beam path.

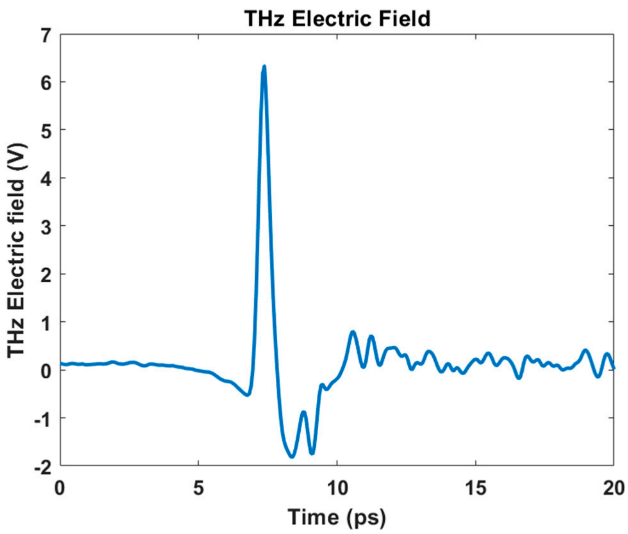

Figure S1. Free space THz electric field vs. time.

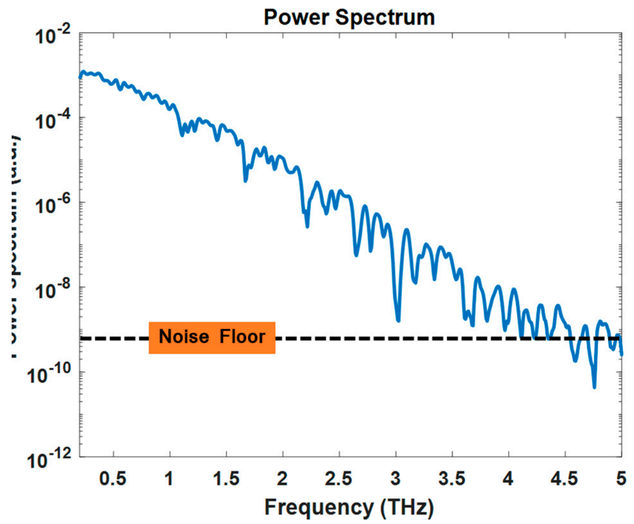

Figure S2. Free space THz power spactrum vs. frequency. The spectral resolution is 15 GHz. The dashed line indicates the noise floor level.

S2. Image Binarization

The image binarization is typically treated as a thresholding operation on a grayscale image [2,3]: the procedure provides to convert a gray scale image into a binary image. In a gray scale image a particular pixel can take an intensity value between 0 to maximum value where in a binary image it could take only two values, either 0 or 1.

There are many binarization methods based on various global and local thresholding operations [2,4-7].

In our case, during the acquisition process of electrical signals, the digitaliation process is made by a 16-bit DAQ board. This imposes the threshold and the gray level resolution to 16 bit. The adopted binarization is linear and the gray levels can vary from 0 to the maximum value $\boldsymbol{M = 2^{16} - 1 = 65535}$.

S3. Image background noise

We studied the background noise as a function of frequency in order to evaluate the process of image formation. Here, we report the pixel histogram distribution for a background image at 1 THz, achieved by blocking the THz radiation with a metallic screen.
The trend of the background curve suggest us the system and also the images are affected by Rayleigh noise [2]. The results are reported in Figure S3.

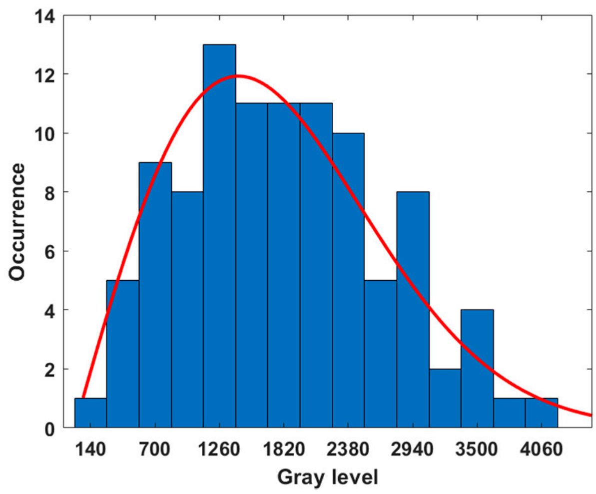

Figure S3. Pixel histogram of background image at 1.0 THz. The red curve fits the blue histogram with the Rayleigh distribution.

Note that, during the acquisition process, images have been digitalised in 16-bit, thus the maximum possible gray level value is $M = 2^{16} - 1 = 65535$ (See section S2). For this reason, as the gray level values in Figure S3 are well below M, they must be considered noise. The histogram is little asymmetrical and can be fitted by the Rayleigh distribution curve $f(x)$. Its mathematical expression is reported below,

$$f(x) = \frac{x-a}{b^2} e^{-\frac{(x-a)^2}{2b^2}} \qquad \text{(S3)}$$

where x corresponds to the gray level values
in Figure S3, while the parameters a and b control the

horizontal shifting and the width of the curve, respectively. The shape is skewed to the right. This trend is confirmed for all the frequencies in our range of interest.

S4. Image signal-to-noise ratio

Our imaging system is characterized by a broadband frequency distribution, from 0.2 to 2.5 THz. The image SNR is then strongly affected by the multi-frequency nature of our source The performances of imaging at different frequencies can be explored by evaluating the image SNR as a function of frequency. A spectral image of a 200 μm pinhole was used. The image SNR can be defined as follows:

$$\boldsymbol{SNR} = \frac{\boldsymbol{\Lambda}}{\boldsymbol{\Sigma}} \qquad \text{(S4)}$$

where **Λ** represent the average signal in a certain region of interest (ROI) and **Σ** the standard deviation of noise in a ROI with the same area [2]. Both **Λ** and **Σ** have been calculated by ImageJ analysis tool.

We calculated the SNR for each image in the range 0.5-2.5 THz. The results are shown in Figure S4.

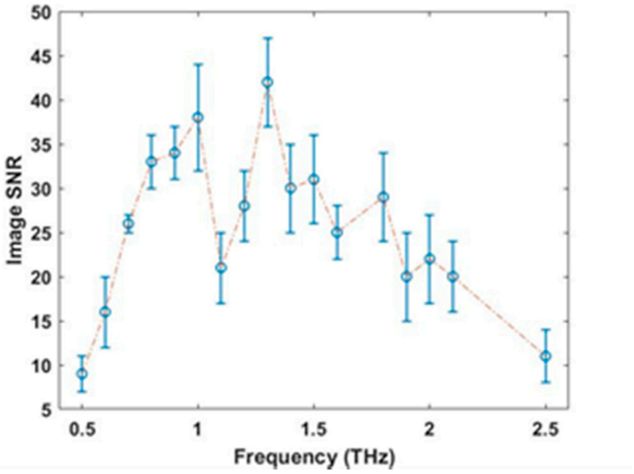

Figure S4. Image signal-to-noise ratio (SNR) as a function of frequency.

The SNR is better for central frequencies, in particular 1 and 1.3 THz. The image acquisition process forces the image dimension to a matrix of N_x x N_y pixels, that is the same for all the spectral images from the same measurement set. Therefore, at lower frequencies (< 0.7 THz), the noise area is very small because the THz spot occupies most of the image. Hence, only few gray levels contribute to the standard deviation evaluation, resulting in high variability and little SNR. At high frequencies (> 2 THz), the image background noise shows high variability because our THz-TDS system SNR is low at those frequencies. As a result, also the image SNR is low. Moreover, the strong THz absorption caused by water vapor results in no image to be shown at 1.7 THz and in the range 2.2-2.4 THz, therefore no image SNR can be calculated. Instead, at 1.1-1.2 THz, where the water vapor absorption is weaker, this only causes an image SNR lowering.

S5. Linen THz transmittance

According to equation (S2), the linen transmittance T as a function of frequency has been calculated and it is reported in Figure S5. Transmittance was used instead of the complex dielectric constant, because the thickness of the textile sample is not well-defined, leading in a great inaccuracy in the calculated complex dielectric constant.

The transmittance shows a cut-off at ~ 1.5 THz. This is in accordance with Naftaly's findings on textile identification with THz-TDS systems [8].

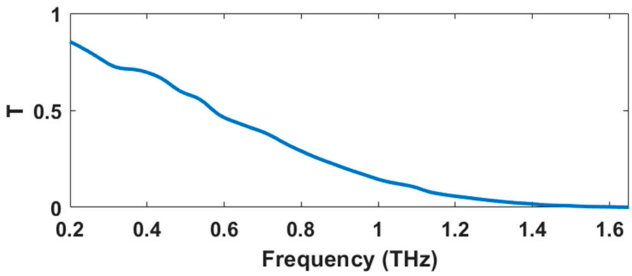

Figure S5. Linen transmittance (T) as a function of frequency. It shows the cut-off at ~ 1.5 THz.

References

1. Zhang, X.C.; Xu, J. *Introduction to THz wave photonics*; Springer, 2010.
2. Gonzalez, R.C.; Woods, R.E. *Digital Image Processing*; Prentice hall New Jersey, 2002.
3. Roy, S.; Saha, S.; Dey, A.; Shaikh, S.H.; Chaki, N. Performance evaluation of multiple image binarization algorithms using multiple metrics on standard image

databases. Proceedings of the 48th Annual Convention of Computer Society of India-Vol II, 2014.
4. Otsu, N. A threshold selection method from gray-level histograms. *IEEE T. Syst. Man. CY-S* **1979**, *9(1)*, 62-6.
5. Niblack, W. *An introduction to Digital Image Processing*; Englewood Cliffs Prentice Hall, 1986.
6. Sezgin, M.; Sankur, B. Survey over image thresholding techniques and quantitative performance evaluation. *J Electron. Imaging* **2004**, *13(1)*,146-66.
7. Shaikh, S.H.; Maiti, A.K.; Chaki, N. A new image binarization method using iterative partitioning. *Mach. Vis. Appl.* **2013**, *24(2)*, 337-50.
8. Naftaly, M.; Molloy, J.; Lanskii, J.; Kokh, K.; Andreev, Y.M. Terahertz time-domain spectroscopy for textile identification. *Appl. Opt.* **2013**, *52(19)*, 4433-7.